Research in Astronomy and Astrophysics, 25:015015 (14pp), 2025 January

https://doi.org/10.1088/1674-4527/ad9b03
CSTR: 32081.14.RAA.ad9b03

Modeling a Relativistic Star in Multi-layered Settings

Avirt S. Lighuda[1] and Alberto K. Mathias[2]
[1] Department of Physics, Mathematics and Informatics, Dar es Salaam University College of Education, 35065, Dar Es Salaam, Tanzania; avirtlighuda@gmail.com
[2] Department of Mathematics and Statistics, The University of Dodoma, 41218, Dodoma, Tanzania; agwaha@gmail.com
Received 2024 October 18; revised 2024 December 01; accepted 2024 December 04; published 2025 January 10

Abstract

This paper yields a new exact solution for dense stellar objects by employing the Einstein–Maxwell system of differential equations. The established model comprises three interior layers with distinguishable equations of state (EoSs): the polytropic EoS at the core layer, the quadratic EoS at the intermediate layer and the modified Van der Waals EoS at the envelope layer. The physical features indicate that the matter variables, metric functions and other physical conditions are viable with dense astrophysical objects. Excitingly, this model is an extension solution of the two-layered model generated by Sunzu and Lighuda. The layers are matched gently across the junctions with the care of the Reissner–Nordström exterior spacetime. Utilizing our model, star masses and radii compatible with observations and satisfactorily known objects are generated. The findings from this paper may be useful to describes purported strange stars such as SAX J1808.4-3658 and binary stars such as Vela X-1.

Key words: stars: interiors – stars: general – stars: massive – stars: neutron

1. Introduction

The establishment of multi-layered stellar models has attracted most researchers in astrophysics and other related areas. A description of a heavier stellar body that has several layers is found in the general theory of relativity, established by Albert Einstein between 1907 and 1916. The theory gives a satisfactory description of the interior structure, focusing on modeling relativistic stellar bodies governed by the set of differential equations. From the general theory of relativity, Einstein field equations are constructed, relating metric functions, energy-density and the momentum tensor. Furthermore, the majority of researchers in astronomy and astrophysics have been utilizing Einstein equations to model relativistic stars with the approach of static or non-static spherically symmetric spacetime (Fulara & Sah 2018). Some studies affirm that the heavier stellar bodies may automatically undergo disintegration after attaining the excited state of collecting cause of transformation (Abreu et al. 2007; Sunzu & Lighuda 2023). Some authors have reported that the collapse of dense objects may result in interstellar bodies that may consolidate to yield a white dwarf state, a neutron star state, or further into black holes (Misner et al. 1973). The studies by Bonnor (1960) and Oppenheimer & Volkoff (1939) show that a dense object can change when the particular thermonuclear point of energy is overly generated at the interior of the stellar sphere. The study by Ipser (1969), who constructed the theory for massive star-gather, indicates that clusters may lead off collapse to produce a black hole. The work of Gedela et al. (2018, 2019, 2021) affirmed that multi-layered stars may comprise complicated interior configurations that need more gravitational explanations. Arrangement of physical quantities inside of the dense objects may result in a series of physical features like energy density, radial and transverse pressures, metric functions, balancing forces and other physical acceptabilities in astrophysical studies (Mafa Takisa et al. 2019; Lighuda et al. 2021a, 2021b, 2023; Sunzu & Lighuda 2023). Many studies were performed consisting of several layers that have been set to explain the interior structure of dense stellar objects. Fewer studies affirm that a composite stellar object may contain sub-layers referred to as core and intermediate that are surrounded by an envelope layer (Pant et al. 2019, 2020, 2021; Bisht et al. 2021; Lighuda et al. 2021a). The inner layer is strongly held by baryon materials, while intermediate and envelope layers are composed of neutron fluids and Coulomb liquids respectively (Gedela et al. 2019; Mafa Takisa et al. 2019; Pant et al. 2020). In the study of astrophysical objects, it is essential to look at the dynamic effect of multi-layered objects for an attentive understanding of the physical features inside the stellar spheres.

Modeling anisotropic stellar objects requires equations of state (EoSs) that should be fixed to explain a particular type of material carried in each layer. EoS is a very important aspect utilized to explain the physical characteristics of the interior layers of the dense star. Several multi-layered models constructed were observed to have a distinguishable EoS in a particular layer relying on the density profile it controlled (Mardan et al. 2021; Sunzu & Lighuda 2023; Mathias et al. 2024a, 2024b). Many studies in general relativity utilize linear EoS, quadratic EoS, polytropic EoS, Chaplygin EoS and the Van der Waals EoS. Some of the models do use an EoS

including the work of Sunzu & Mashiku (2018), Ngubelanga & Maharaj (2015), Pant et al. (2019, 2020), Lighuda et al. (2021a, 2021b), Bisht et al. (2021), Rahaman et al. (2010), Mafa Takisa & Maharaj (2016), Mafa Takisa et al. (2019), Gedela et al. (2019), Maharaj & Mafa Takisa (2013), Ngubelanga et al. (2015), Komathiraj & Maharaj (2007), and Kumar et al. (2019).

Inclusion of charge in the construction of anisotropic stellar models assists in giving stimulative physical features (Bhatia et al. 1969). Gravitating objects may abruptly gain or loose charge in their position in the Universe. The availability of charge inside the multi-layered sphere assists in balancing the gravitational field (Malaver 2017a, 2017b). Some researchers have reported that the existence of charge enhances the balance of stellar bodies versus gravitational breakdown, increases the mass and central curvature, and affects the redshift, compaction and luminosity of stellar bodies (Varela et al. 2010; Mardan et al. 2021). The effect of electric field in the study of multi-layered stars has also been investigated in the works of Maharaj et al. (2014), Sunzu et al. (2014a, 2014b, 2019), Sharma & Maharaj (2007), Rahaman et al. (2010), Lighuda et al. (2021a, 2021b), Lighuda et al. (2023), Sunzu & Lighuda (2023) and Mafa Takisa & Maharaj (2016).

The existence of pressure anisotropy in the interior of a stellar body has been demonstrated and discussed in many relativistic models (Murad 2016; Maurya et al. 2022). It has been reported that the availability of pressure in the interior of a stellar sphere relies on the flowing matter configuration (Maurya & Ortiz 2019). Fewer authors have asserted that it is not necessary for pressure to comply with the isotropic limit ($p_r = p_t$), instead, anisotropic criteria ($p_r \neq p_t$) may bring affect how the compact structures of dense stellar spheres like neutron stars, white dwarfs and black holes appear (Komathiraj & Maharaj 2007; Thirukkanesh & Maharaj 2009; Bijalwan 2011). The work of Makalo et al. (2022) addressed the fact that pressure anisotropy could provide a variety of physical features due to a tough core, by the existence of superfluid, or by distinct transitions. The studies by Maurya & Ortiz (2019), Maurya et al. (2022) affirmed that when the pressure anisotropy is positive (i.e., $\Delta = p_t - p_r > 0$), the stellar body experiences repulsion and if it is negative (i.e., $\Delta = p_t - p_r < 0$), this results in attraction. Additionally, a positive measure of anisotropy helps to keep the stability and equalize the matter configuration inside of the stellar sphere. Some of the anisotropic models that describe the feasibility of pressure in general relativity include the work of Bijalwan (2011), Komathiraj & Maharaj (2007), Bhar et al. (2017), Maharaj & Mafa Takisa (2013), Mathias et al. (2021) and Maurya et al. (2022).

Models that consist of multi-layers have been established regarding the inner and outer layers by employing the Einstein–Maxwell system of equations including EoSs. Recently, two-layered models formulated include the works of Mathias et al. (2024a, 2024b), Sunzu & Lighuda (2023) and Mardan et al. (2021) who inserted EoSs in the respective layers. The studies by Mafa Takisa & Maharaj (2016) and Mafa Takisa et al. (2019) developed models by substituting a linear EoS at the core and quadratic EoS at the envelope: results show that the envelope layer has the least concentration compared to the core layer. Thomas et al. (2005) constructed a stellar model that comprises an isotropic fluid state in the core layer and an anisotropic fluid state from the envelope layer. Tikekar & Jotania (2009) developed a relativistic model with anisotropic matter distributed in the core and isotropic matter in the envelope layer. The model formulated by Metcalfe et al. (2003) gives deep descriptions of the physical features of white dwarf objects. The works of Pant et al. (2019) and Gedela et al. (2018, 2019, 2021) elaborate on the feasibility of geometrical features of dense objects by applying a linear EoS in the core and quadratic EoS in the envelope layer. Similar features for two-layer models are also demonstrated in the works of Sharma & Mukherjee (2002), Hansraj et al. (2016), Montgomery et al. (2003), Tikekar & Jotania (2009), Ramesh & Thomas (2005) and Sunzu et al. (2019).

In a study of relativistic objects, fewer three-layered models have been constructed regarding density visibility from each layer. Some of the three-layered stellar models are found with the absence of an electric field describing the layers. The three-layered models developed by Bisht et al. (2021), Gedela et al. (2021), and Pant et al. (2020) have demonstrated and discussed the physical characteristics and geometrical features of uncharged neutron stars. On the other hand, the charged core-intermediate-envelope models formulated by Lighuda et al. (2021a, 2021b) and Lighuda et al. (2023) have remarked on the physical properties of the massive objects and highlighted the importance of electric charge in the construction of the three-layered models.

This study aims to develop a charged three-layered model as an extension of the two-layered model constructed by Sunzu & Lighuda (2023). Our model comprises distinct layers: The core layer is fitted with a polytropic EoS, an intermediate layer is described by a quadratic EoS and the envelope obeys a modified Van der Waals EoS. The work by Olengeile et al. (2023) generated a three-layered model where the Van dar Waals EoS is inserted at the intermediate layer. The work by Lighuda et al. (2021a) developed the three-layered models by utilizing a linear EoS at the core, quadratic EoS at the intermediate and Chaplygin EoS at the envelope region. The model by Lighuda et al. (2023) utilized a polytropic EoS at the core, quark matter at intermediate, and Chaplygin EoS at the envelope layer. A remarkable aspect of our paper is the third layer fitted with the Van dar Waals EoS, a significant feature that distinguishes this work from Lighuda et al. (2021a, 2023), Olengeile et al. (2023) and Sunzu & Lighuda (2023). The geometrical features of the three-layered model are subsequently observed.

To develop a relativistic stellar model, we regard a static spherically symmetric spacetime described using Schwarzschild coordinates ($x^{\iota} = t, r, \theta, \phi$) as

$$ds^2 = -e^{\nu(r)}dt^2 + e^{\lambda(r)}dr^2 + r^2(d\theta^2 + \sin^2\theta d\phi^2). \quad (1)$$

The basic line element describing the exterior spacetime for a charged object is expressed in terms of Reissner–Nordström geometry

$$ds^2 = -\left(1 - \frac{2M}{r} + \frac{Q^2}{r^2}\right)dt^2 + \left(1 - \frac{2M}{r} + \frac{Q^2}{r^2}\right)^{-1}dr^2 + r^2(d\theta^2 + \sin^2\theta d\phi^2), \quad (2)$$

where $\nu(r)$ and $\lambda(r)$ define the metric functions, Q stands for total charge and ϵ expresses the total mass of the object. The energy-momentum tensor for the charged body is regarded as

$$\Lambda_{ij} = \text{diag}\left(-\rho - \frac{1}{2}E^2, p_r - \frac{1}{2}E^2, p_t + \frac{1}{2}E^2, p_t + \frac{1}{2}E^2\right), \quad (3)$$

where ρ expresses energy density, E is electric field, and p_r and p_t denote radial and transverse pressures as well. If $G = c = 1$ are set due to geometrical reasons, the Einstein–Maxwell field equations may be expressed in the form

$$8\pi\rho + \frac{1}{2}E^2 = \frac{1}{r^2}(1 - e^{-2\lambda}) + \frac{2\lambda'}{r}e^{-2\lambda}, \quad (4a)$$

$$8\pi p_r - \frac{1}{2}E^2 = -\frac{1}{r^2}(1 - e^{-2\lambda}) + \frac{2\nu'}{r}e^{-2\lambda}, \quad (4b)$$

$$8\pi p_t + \frac{1}{2}E^2 = e^{-2\lambda}\left(\nu'' + \nu'^2 - \nu'\lambda' + \frac{\nu'}{r} - \frac{\lambda'}{r}\right) + \frac{2\lambda'}{r}e^{-2\lambda}, \quad (4c)$$

$$\sigma = \frac{1}{r^2}e^{-\lambda}(r^2E)', \quad (4d)$$

where primes ($'$ and $''$) signify the first and second derivatives respectively.

In our study, we transform and simplify the system of field equations by utilizing the new variables obtainable in Durgapal & Bannerji (1982, 1983) written in the form

$$x = r^2, \quad Z(x) = e^{-\lambda}, \quad e^{2\nu} = A^2y^2(x). \quad (5)$$

Putting Equation (5) in the system of differential equations (4), the transformed system of field equations is expressed as

$$\rho = \frac{1}{8\pi}\left(\frac{1 - Z}{x} - 2\frac{dZ}{dx} - \frac{1}{2}E^2\right), \quad (6a)$$

$$p_r = \frac{1}{8\pi}\left(-\frac{1}{x}(1 - Z) + 4Z\frac{1}{y}\frac{dy}{dx} + \frac{1}{2}E^2\right), \quad (6b)$$

$$p_t = \frac{1}{8\pi}\left(4xZ\frac{1}{y}\frac{d^2y}{dx^2} + \left(4Z + 2x\frac{dZ}{dx}\right)\frac{1}{y}\frac{dy}{dx} + \frac{dZ}{dx} - \frac{1}{2}E^2\right), \quad (6c)$$

$$\Delta = 8\pi(p_t - p_r), = \frac{1}{8\pi}\left(4xZ\frac{\ddot{y}}{y} + \left(4xZ + 2x\frac{dZ}{dx} - 4Z\right)\frac{\dot{y}}{y} + \frac{dZ}{dx} + \frac{1}{x}(1 - Z) - E^2\right), \quad (6d)$$

$$\sigma = 2\left(x\frac{dE}{dx} + E\right)\sqrt{\frac{Z}{x}}. \quad (6e)$$

The system of differential equations (6) has eight undetermined parameters (ρ, p_t, p_r, Δ, Z, y, σ, E). To solve the system (6), one may specify any of the two physical parameters to yield solutions of the other parameters.

Based on physical grounds, one of the metric functions used in the work of Lighuda et al. (2021b) and Sunzu & Lighuda (2023) has been applied to formulate a core- intermediate-envelope model to extend the work of Sunzu & Lighuda (2023). This is written as

$$Z(x) = e^{-\lambda} = 1 - \zeta x + \varepsilon x^2, \quad (7)$$

where ζ and ε are the arbitrary real constants. The selected metric function Z satisfies regularity and continuity throughout the stellar interior. When we set $\zeta = \varepsilon = 0$, the metric function (7) is observed to be non-zero which is physically reasonable in the study of relativistic stellar objects (Sunzu & Lighuda 2023). The metric function Z expressed in Equation (7) is finite, indicating that no discontinuity point can be observed as one runs away from the center.

In our solution, we regard the electric field as described in the works of Lighuda et al. (2021b) and Sunzu & Lighuda (2023), written as

$$E^2 = \vartheta xZ = x\vartheta(1 - \zeta x + \varepsilon x^2), \quad (8)$$

where ϑ is an arbitrary real constant. The selected electromagnetic field E^2 in Equation (8) is feasible, finite and continuous and may be observed running away to the surface. Applying $\vartheta = 0$ in (8), our solutions may revert back to earlier uncharged multi-layered stellar models (Gedela et al. 2019; Pant et al. 2020; Bisht et al. 2021). In our study, we opted to adopt the metric function and electric field from the previous study since they are free from geometrical singularities and they describe realistic stellar models with astrophysical significance.

2. Categorization of the Interior Regions

The interior layers of the dense objects are sequentially specified into three cases: the core (a), intermediate (b) and envelope (c). These regions are defined by the core (Region a): $0 \leqslant r \leqslant R_a$, (0−2.5) km, intermediate (Region b): $R_a \leqslant r \leqslant R_b$, (2.5–6) km, and envelope layers (Region c): $R_b \leqslant r \leqslant R_c$, (6–10) km.

The basic line element (1) is now expressed in three layers as

$$ds^2|_a = -e^{\nu_a}dt^2 + e^{\lambda_a}dr^2 + r^2(d\theta^2 + \sin^2\theta d\phi^2), \quad (9a)$$

$$ds^2|_b = -e^{\nu_b}dt^2 + e^{\lambda_b}dr^2 + r^2(d\theta^2 + \sin^2\theta d\phi^2), \quad (9b)$$

$$ds^2|_c = -e^{\nu_c}dt^2 + e^{\lambda_c}dr^2 + r^2(d\theta^2 + \sin^2\theta d\phi^2). \quad (9c)$$

2.1. Region a (Core Layer)

The fundamental hypothesis of polytropes affirms that the pressure inside the sphere is normally countered by the force of gravity which depends on the density profile. The core layer is compact, consisting of the solid matter configuration. The polytropic EoS is applied in the core layer since it is convenient to explain the solid materials (Mardan et al. 2021; Lighuda et al. 2023; Sunzu & Lighuda 2023). Notable here is the geometrical features that may have resulted from polytropes. This EoS is given as

$$p_{r_a} = \upsilon\rho_a^{1+1/n}, \quad (10)$$

where υ and n correspond to arbitrary real constants, meeting the condition $n > 0$. Placing (6a) in (10) results in

$$p_{r_a} = \upsilon\left(\frac{1-Z}{8\pi x} - \frac{dZ}{4\pi dx} - \frac{1}{16\pi}E^2\right)^{1+1/n}. \quad (11)$$

Equations (6b) and (11) are equated to give

$$\frac{1}{y}\frac{dy}{dx} = \frac{\upsilon}{4Z}\left(\frac{1-Z}{8\pi x} - \frac{dZ}{4\pi dx} - \frac{1}{16\pi}E^2\right)^{1+1/n} + \frac{1-Z}{4Zx} - \frac{E^2}{8Z}. \quad (12)$$

Assembling (7) and (8) into Equation (12) results in the differential equation

$$\frac{1}{y}\frac{dy}{dx} = \frac{1}{8}\left(\frac{-x\vartheta + 2(\zeta - x\varepsilon)}{1 - x\zeta + x^2\zeta} + 2^{-3-4/n}\pi^{-((1+n)/n)} \times (1 - x\zeta + x^2\xi)(\zeta(6 + x^2\vartheta) - x(\vartheta + 10\varepsilon + x^2\varepsilon\vartheta))^{1+1/n}\upsilon)\right). \quad (13)$$

Applying Equations (7), (8), and (13) and the system of differential equations (6), the metric functions and matter variables of the core layer are obtainable in the form

$$e^{\lambda_a} = [1 - \zeta x + \varepsilon x^2]^{-1}, \quad (14a)$$

$$e^{\nu_a} = A^2[\exp(S_0(x))]^2, \quad (14b)$$

$$\rho_a = (\zeta(4 + 2x + x^2\vartheta) - x(\vartheta + 2(4 + x)\varepsilon + x^2\vartheta\varepsilon))(16\pi)^{-1}, \quad (14c)$$

$$p_{r_a} = (16\pi)^{-((1+n)/n)}(\zeta(4 + 2x + x^2\vartheta) - x(\vartheta + 2(4 + x)\xi + x^2\vartheta\varepsilon))^{1+1/n}\upsilon, \quad (14d)$$

$$p_{t_a} = \tfrac{1}{64}(-8\vartheta + (16(\zeta - 2x\varepsilon)(\zeta - x\varepsilon))/(1 - x\zeta + x^2\varepsilon)^2 - (16\varepsilon)/(1 - x\zeta + x^2\varepsilon) + 2^{-4/n}\pi^{-((1+n)/n)}(-\zeta + 2x\varepsilon)(\zeta(6 + x^2\vartheta) - x(\vartheta + 10\varepsilon + x^2\vartheta\varepsilon))^{1+1/n}\upsilon - (2^{-4/n}(1 + n)\pi^{-((1+n)/n)}(1 - x\zeta + x^2\varepsilon) \times (\vartheta - 2x\zeta\vartheta + 10\varepsilon + 3x^2\vartheta\varepsilon)(\zeta(6 + x^2\vartheta) - x(\vartheta + 10\varepsilon + x^2\vartheta\xi))^{1/n}\upsilon)/n + (-x\vartheta + (2(\zeta - x\xi))/(1 - x\zeta + x^2\varepsilon) + 2^{-3-4/n} \times \pi^{((-1-n)/n)}(1 - x\zeta + x^2\varepsilon)(\zeta(6 + x^2\vartheta) - x(\vartheta + 10\varepsilon + x^2\vartheta\varepsilon))^{1+1/n}\upsilon)^2), \quad (14e)$$

$$\Delta_a = p_{t_a} - p_{r_a}, \quad (14f)$$

$$\sigma_a = 2\sqrt{1/x - \zeta + x\varepsilon}\,(x\vartheta(1 - x\zeta + x^2\varepsilon) + \tfrac{1}{2}\left(3 + \tfrac{-2 + x\zeta}{1 - x\zeta + x^2\varepsilon}\right)\Big), \quad (14g)$$

$$E_a^2 = \vartheta x(1 - \zeta x + \varepsilon x^2), \quad (14h)$$

where for ease, we have stated

$$S_0(x) = \tfrac{1}{8}\int_0^{2.5}(-x\vartheta + (2(\zeta - x\varepsilon))/(1 - x\zeta + x^2\varepsilon) + 2^{-3-4/n}\pi^{-((1+n)/n)}(1 - x\zeta + x^2\varepsilon)(\zeta(6 + x^2\vartheta) - x(\vartheta + 10\varepsilon + x^2\vartheta\varepsilon))^{1+1/n}\upsilon)dx.$$

In the core layer, the sum of the mass is expressed in the form

$$M_a(r) = 4\pi\int_0^r r^2\rho_a dr, \quad r^2 = x$$

$$M_a(x) = (x^{3/2}(42(10 + 3x)\zeta + 9x(-7 + 5x\zeta)\vartheta - x(504 + 5x(18 + 7x\vartheta))\varepsilon))(1260)^{-1} + c_0, \quad (15)$$

where c_0 stands for an integration constant.

2.2. Region b (Intermediate Layer)

Here, a quadratic EoS is inserted between to describe the physical trends of the matter arrangement in the intermediate layer that is characterized by less fused substances, namely neutron fluids and Coulomb liquids. The quadratic EoS is assigned to emphasize that the radially directed force in the intermediate layer is less than in the core layer (Lighuda et al. 2021b; Sunzu & Lighuda 2023). This is written as

$$p_{r_b} = L\rho_b^2 + N\rho_b - \Upsilon, \quad (16)$$

note that L, N and Υ are arbitrary real constants.

Regarding Equations (6a) and (16), we have acquired

$$p_{r_b} = L\left(\frac{1-Z}{8\pi x} - \frac{dZ}{4\pi dx} - \frac{1}{16\pi}E^2\right)^2 + N\left(\frac{1-Z}{8\pi x} - \frac{dZ}{4\pi dx} - \frac{1}{16\pi}E^2\right) - \Upsilon. \quad (17)$$

Combining Equations (6b) and (17), and making use of Equations (7) and (8), we produce a differential equation in the form

$$\begin{aligned}\frac{1}{y}\frac{dy}{dx} &= (-128\pi^2(2\Upsilon + x\vartheta + (2 + x^2\vartheta)(-\zeta + x\xi)) \\ &+ 16\pi N(\zeta(6 + x^2\vartheta) \\ &- x(\vartheta + 10\varepsilon + x^2\vartheta v)) \\ &+ (\zeta(6 + x^2\vartheta) - x(\vartheta + 10\varepsilon \\ &+ x^2\vartheta\varepsilon))^2 L)(1024\pi^2(1 - x\zeta + x^2\varepsilon))^{-1}. \end{aligned} \quad (18)$$

Plugging (7), (8), and (18) into the field equation (6), matter variables and metric functions are obtainable as

$$e^{\nu_b} = A^2 y^2(x) = A^2[\exp(S_1(x))]^2\,, \quad (19a)$$

$$\rho_b = (\zeta(4 + 2x + x^2\vartheta) - x(\vartheta + 2(4 + x)\varepsilon + x^2\vartheta\xi))(16\pi)^{-1}, \quad (19b)$$

$$\begin{aligned} p_{r_b} &= L[(\zeta(4 + 2x + x^2\vartheta) - x(\vartheta + 2(4 + x)\varepsilon + x^2\vartheta\varepsilon)) \\ &\times (16\pi)^{-1}]^2 N[(\zeta(4 + 2x + x^2\vartheta) \\ &- x(\vartheta + 2(4 + x)\varepsilon + x^2\vartheta\varepsilon)) \\ &\times (16\pi)^{-1}] - \Upsilon, \end{aligned} \quad (19c)$$

$$\begin{aligned} p_{t_b} &= (\zeta - 2x\varepsilon)(8\pi)^{-1} - (x\vartheta(1 - x\zeta + x^2\varepsilon))(16\pi)^{-1} \\ &+ ((2 - 3x\zeta + 4x^2\varepsilon)(-128\pi^2(2\Upsilon \\ &- \zeta(2 + x^2\vartheta) + x(\vartheta + 2\xi + x^2\vartheta\varepsilon)) \\ &+ 16\pi N(\zeta(6 + x^2\vartheta) - x(\vartheta + 10\varepsilon + x^2\vartheta)) \\ &+ (\zeta(6 + x^2\vartheta) - x(\vartheta + 10\varepsilon + x^2\vartheta\varepsilon))^2 L)) \\ &\times (4096\pi^3(1 - x\zeta + x^2\xi))^{-1} + (1/(2097152\pi^5(1 \\ &- x\zeta + x^2\varepsilon)))x(-1024\pi^2(16\pi N(\zeta^2(-6 + x^2\vartheta) \\ &- 10\varepsilon(-1 + x^2\xi) + \vartheta(1 + x^2\varepsilon)^2 - 2x\zeta(\vartheta \\ &- 6\varepsilon + x^2\vartheta\varepsilon)) + 128\pi^2(\zeta^2(-2 + x^2\vartheta) \\ &+ \vartheta(1 + x^2\varepsilon)^2 - 2\xi(-1 + 2x\Upsilon + x^2\varepsilon) + 2\zeta(\Upsilon \\ &- x(\vartheta - 2\varepsilon + x^2\vartheta\varepsilon))) + (\zeta(-6\zeta + x(-5 + 3x\zeta)\vartheta) \\ &+ x(6x\vartheta + \zeta(2 - 7x^2\vartheta))\varepsilon + 4x^4\vartheta\varepsilon^2 \\ &+ 2(\vartheta + 10\varepsilon))(\zeta(6 + x^2\vartheta) - x(\vartheta + 10\varepsilon + x^2\vartheta\varepsilon))L) \\ &+ (-128\pi^2(2G + x\vartheta + (2 + x^2\vartheta)(-\zeta + x\varepsilon)) \\ &+ 16\pi N(\zeta(6 + x^2\vartheta) - x(\vartheta + 10\varepsilon + x^2\vartheta\varepsilon)) + (\zeta(6 + x^2\vartheta) \\ &- x(\vartheta + 10\varepsilon + x^2\vartheta\varepsilon))^2 L)^2), \end{aligned} \quad (19d)$$

$$\Delta_b = p_{t_b} - p_{r_b}, \quad (19e)$$

note that

$$\begin{aligned} S_1(x) &= -(1/(61440\pi^2))(x(5xL\vartheta(72\zeta + x(-4 + 3x\zeta)\vartheta) \\ &- 4L(1500 + x^2\vartheta(100 + 3x^2\vartheta))\varepsilon \\ &+ 2097152\pi^5 \quad N(-20\zeta^2(18 + x^2\vartheta) \\ &+ \zeta(720(1 + \Upsilon) + 12x^4\vartheta^2 + 15x^3\vartheta(\varepsilon + \vartheta) \\ &+ 20x^2\vartheta(8 + 2\Upsilon - \varepsilon) + 30x(6\varepsilon + 7\vartheta + 10\varepsilon)) \\ &+ x(-200(3 + x\varepsilon + 3\Upsilon)\varepsilon + 5\vartheta(-4(3 \\ &+ x\varepsilon + 3\Upsilon) + x(3x(-10 + \varepsilon) + 8(-4 + \Upsilon))\varepsilon) \\ &+ x\vartheta^2(-20 + 3x(-5 + 5\varepsilon + 4x\varepsilon))))) \\ &+ 240L(13\zeta^2 - 50v)\arctan(\zeta \\ &- 2x\varepsilon)/(-\zeta^2 + 4\varepsilon)^{1/2}/(-\zeta^2 + 4\varepsilon)^{1/2} \\ &+ 600L\zeta\log 1 - x\zeta + x^2\varepsilon. \end{aligned}$$

The total mass of a stellar object in the intermediate layer is written in the form

$$\begin{aligned} M_b(r) &= 4\pi\int_0^r r^2\rho_a dr, \quad r^2 = x \\ M_b(x) &= (x^{3/2}(42(10 + 3x)\zeta + 9x(-7 + 5x\zeta)\vartheta \\ &- x(504 + 5x(18 + 7x\vartheta))\varepsilon))(1260)^{-1} + c_1, \end{aligned} \quad (20)$$

where c_1 denotes an integration constant.

2.3. Region c (Envelope Layer)

The envelope layer may be considered as a gaseous matter that has the lowest density of all layers. We insert the modified Van der Waals EoS that is adequately countable to describe the outermost layer (Malaver 2017a, 2017b). This is written as

$$p_{r_c} = \alpha\rho_c^{\omega+1} + \frac{\beta\rho^\omega}{1 + \gamma\rho_c^\omega}, \qquad \omega = 1/n \quad (21)$$

where α, β and γ are arbitrary real constants. The energy density and radial pressure are subsequently respectively given by

$$\rho_c = \frac{1-Z}{x} - 2\frac{dZ}{dx} + \frac{1}{2}E^2, \quad (22)$$

and

$$p_{r_a} = -\frac{1-Z}{x} + 4Z\frac{1}{y}\frac{dy}{dx} + \frac{E^2}{2}. \quad (23)$$

Plugging Equation (22) into (21) yields

$$p_{r_c} = \alpha\left(\frac{1-Z}{x} - 2\frac{dZ}{dx} + \frac{E^2}{2}\right)^{\omega+1} - \beta\left(\frac{1-Z}{x} - 2\frac{dZ}{dx} + \frac{E^2}{2}\right)^{\omega} \times \left(1 + \left(\frac{1-Z}{x} - 2\frac{dZ}{dx} + \frac{E^2}{2}\right)^{\omega}\right)^{-1}. \quad (24)$$

Regarding Equations (23) and (24), the results are

$$\frac{1}{y}\frac{dy}{dx} = \frac{1}{4Z}\left(\frac{1-Z}{x} + \frac{E^2}{2}\right) + \frac{\alpha}{4Z}\left(\frac{1-Z}{x} - 2\frac{dZ}{dx} + \frac{E^2}{2}\right)^{\omega+1} - \frac{\beta}{4Z}\left(\frac{1-Z}{x} - 2\frac{dZ}{dx} + \frac{E^2}{2}\right)^{\omega} \times \left(1 + \left(\frac{1-Z}{x} - 2\frac{dZ}{dx} + \frac{E^2}{2}\right)^{\omega}\right)^{-1}. \quad (25)$$

Employing the chosen metric function Z and the electric field E^2, we have arrived at a differential equation in the form

$$\frac{1}{y}\frac{dy}{dx} = (\zeta - x\varepsilon + 1/2x\vartheta(1 - x\zeta + x^2\varepsilon) + \alpha(3\eta - 5x\varepsilon + 1/2x\vartheta(1 - x\zeta + x^2\varepsilon))^(1 + \omega) + \beta(-1 + 1/(1 + (3\zeta - 5x\varepsilon + 1/2x\vartheta(1 - x\zeta + x^2\varepsilon))^{\omega})))/(4(1 - x\zeta + x^2\varepsilon)). \quad (26)$$

Solving Equation (26), the matter variables and metric functions of the envelope layer are obtainable as

$$e^{\lambda_c} = [1 - \zeta x + \varepsilon x^2]^{-1}, \quad (27a)$$

$$e^{2\nu_c} = A^2 y^2(x) = A^2[\exp(S_2(x))]^2, \quad (27b)$$

$$\rho_c = (3\zeta - 5x\varepsilon + 1/2x\vartheta(1 - x\zeta + x^2\varepsilon))/(8\pi), \quad (27c)$$

$$p_{r_c} = (8^{-\omega-2}((3\zeta - 5x\varepsilon + 1/2x\vartheta(1 - x\zeta + x^2\varepsilon))/\pi)^{\omega}((\alpha(3\zeta - 5x\varepsilon + 1/2x\mu(1 - x\zeta + x^2\varepsilon)))/\pi + (\beta 8^{\omega+1})/(8^{\omega} + ((3\zeta - 5x\varepsilon + 1/2x\vartheta(1 - x\zeta + x^2\varepsilon))/\pi)^{\omega})))/\pi, \quad (27d)$$

$$p_{t_c} = 4 - \zeta - 4x\zeta + 2x\varepsilon + 4x^2\varepsilon - 1/2x\mu(1 - x\zeta + x^2\varepsilon) + (x(-\zeta + 2x\varepsilon)(\zeta - x\varepsilon + 1/2x\vartheta(1 - x\zeta + x^2\varepsilon) + \alpha(3\eta - 5x\varepsilon + 1/2x\vartheta(1 - x\zeta + x^2\varepsilon))^{1+\omega} + \beta(-1 + 1/(1 + (3\zeta - 5x\varepsilon + 1/2x\vartheta(1 - x\zeta + x^2\varepsilon))^{\omega})))/(2(1 - x\zeta + x^2\varepsilon)) + (1/(32\pi(1 - x\zeta + x^2\varepsilon))) \times (4(-\zeta + 2x\varepsilon)(\zeta - x\varepsilon + 1/2x\vartheta(1 - x\zeta + x^2\varepsilon) + \alpha(3\zeta - 5x\varepsilon + 1/2x\vartheta(1 - x\zeta + x^2\varepsilon))^{1+\omega} + \beta(-1 + 1/(1 + (3\zeta - 5x\varepsilon + 1/2x\vartheta(1 - x\zeta + x^2\varepsilon))^{\omega}))) + (\zeta - x\varepsilon + 1/2x\vartheta(1 - x\zeta + x^2\varepsilon) + \alpha(3\zeta - 5x\varepsilon + 1/2x\vartheta(1 - x\zeta + x^2\varepsilon))^{1+\omega} + \beta(-1 + 1/(1 + (3\zeta - 5x\varepsilon + 1/2x\vartheta(1 - x\zeta + x^2\varepsilon))^{\omega})))^2 + 2(1 - x\zeta + x^2\varepsilon)(-2\varepsilon + x\vartheta(-\zeta + 2x\varepsilon) + \vartheta(1 - x\zeta + x^2\varepsilon) - (\beta(\vartheta - 2x\zeta\vartheta - 10\varepsilon + 3x^2\vartheta\varepsilon)(3\zeta - 5x\varepsilon + 1/2x\vartheta(1 - x\zeta + x^2\varepsilon))^{-1+\omega}\omega)/(1 + (3\zeta - 5x + 1/2x\vartheta(1 - x\zeta + x^2\varepsilon))^{\omega})^2 + \alpha(\vartheta - 2x\zeta\vartheta - 10\varepsilon + 3x^2\vartheta\varepsilon)(3\zeta - 5x\varepsilon + 1/2x\vartheta(1 - x\zeta + x^2\varepsilon))^{\omega}(1 + \omega))), \quad (27e)$$

$$\Delta_c = p_{t_c} - p_{r_c}, \quad (27f)$$

$$\sigma_c = 2(1/x - \zeta + x\varepsilon)^{1/2}(x\vartheta(1 - x\zeta + x^2\varepsilon) + \frac{1}{2}\left(3 + \frac{-2 + x\zeta}{1 - x\zeta + x^2\xi}\right)), \quad (27g)$$

$$E_c^2 = \vartheta x(1 - \zeta x + \varepsilon x^2), \quad (27h)$$

where

$$S_2(x) = \int_6^{10} ((\zeta - x\varepsilon + 1/2x\vartheta(1 - x\zeta + x^2\varepsilon) + \alpha(3\eta - 5x\varepsilon + 1/2x\vartheta(1 - x\zeta + x^2\varepsilon))^{1+\omega} + \beta(-1 + 1/(1 + (3\zeta - 5x\varepsilon + 1/2x\vartheta(1 - x\zeta + x^2\varepsilon))^{\omega})))/(4(1 - x\zeta + x^2\varepsilon)))dx.$$

The envelope layer composed of a gaseous fluid has total mass written in the form

$$M_c(r) = 4\pi \int_0^r r^2 \rho_a dr, \quad r^2 = x$$
$$M_c(x) = (x^{3/2}(42(10 + 3x)\zeta + 9x(-7 + 5x\zeta)\vartheta - x(504 + 5x(18 + 7x\vartheta))\varepsilon))(1260)^{-1} + c_2, \quad (28)$$

where c_2 denotes an integration constant.

3. Matching Conditions

When trying to satisfy continuity, the matching of the radial pressure and metric functions should meet the requirements at the interface of the star boundary. The matching rules may be stipulated as:

The junction criterion at the core-intermediate

$$e^{\lambda_a}(R_a) = e^{\lambda_b}(R_a), \quad (29a)$$

$$e^{\nu_a}(R_a) = e^{\nu_b}(R_a), \quad (29b)$$

$$p_{r_a}(R_a) = p_{r_b}(R_a). \quad (29c)$$

The junction criterion at the intermediate-envelope

$$e^{\lambda_b}(R_b) = e^{\lambda_c}(R_b), \quad (30a)$$

$$e^{\nu_b}(R_b) = e^{\nu_c}(R_b), \quad (30b)$$

$$p_{r_b}(R_b) = p_{r_c}(R_b). \quad (30c)$$

The junction criterion at the envelope-surface needs the interior and exterior line elements (1) and (2) to match gently at the interface $r = R_c$. We get

$$e^{\lambda_c}(R_c) = \left(1 - \frac{2M}{R_c} + \frac{Q^2}{R_c^2}\right)^{-1}, \quad (31a)$$

$$e^{\nu_c}(R_c) = \left(1 - \frac{2M}{R_c} + \frac{Q^2}{R_c^2}\right), \quad (31b)$$

$$p_{r_c}(R_c) = 0. \quad (31c)$$

Substituting the required equations yields

$$(1 + \zeta R_c^2 + \varepsilon R_c^2) = H_1(x), \quad (32a)$$

$$A^2[\exp(S_2(x))]^2 = H_2(x), \quad (32b)$$

$$(8^{-\omega-2}((3\zeta - 5x\varepsilon + 1/2x\vartheta(1 - x\zeta = H_3(x),$$

Table 1
Stellar Masses and Radii Consistent with Other Findings

$\zeta(10^{-3})$	$\vartheta(10^{-5})$	$\varepsilon(10^{-1})$	R	$M/M_\odot$	Model Applied
2.0	6.85	6.75	9.17	1.27	Mathias et al. (2024a)
2.2	6.88	6.79	9.0	0.81	Maurya et al. (2022)
2.4	6.90	7.2	9.81	1.65	Sunzu & Lighuda (2023)
2.6	7.1	7.5	8.5	0.79	Ngubelanga & Maharaj (2015)
2.8	7.4	7.8	8.27	0.74	Mafa Takisa et al. (2019)
3.0	7.7	8.1	9.28	1.15	Ngubelanga & Maharaj (2015)
3.2	7.8	8.4	7.47	0.88	Lighuda et al. (2021a)
3.4	8.0	8.7	6.65	1.33	Ngubelanga et al. (2015)

Table 2
Masses for Specific Stars

$\zeta(10^{-3})$	$\vartheta(10^{-5})$	$\varepsilon(10^{-1})$	R	$M/M_\odot$	Star
2.0	6.85	6.75	9.17	1.27	SAX J1808.4-3658
2.2	6.88	6.79	9.0	0.81	Her X-1
2.4	6.90	7.2	9.81	1.65	4U 1538-52
2.6	7.1	7.5	8.5	0.79	PRS J1614-2230
2.8	7.4	7.8	8.27	0.74	LMC-X-4
3.0	7.7	8.1	9.28	1.15	RX J1856-37
3.2	7.8	8.4	7.47	0.88	Cen X-3
3.4	8.0	8.7	6.65	1.33	EXO 1785-248

note that for easy viewing we have put

$$H_0(x) = (x^{3/2}(42(10 + 3x)\zeta + 9x(-7 + 5x\zeta)\vartheta - x(504 + 5x(18 + 7x\vartheta))\varepsilon))(1260)^{-1} + c_2,$$
$$H_1(x) = \left(1 - \frac{2H_0(x)}{R_c} + \frac{\vartheta R_c(1 - \zeta R_c + \varepsilon R_c^2)}{R_c^2}\right)^{-1},$$
$$H_2(x) = 1 - \frac{2H_0(x)}{R_c} + \frac{\vartheta R_c(1 - \zeta R_c + \varepsilon R_c^2)}{R_c^2},$$
$$H_3(x) = +x^2\varepsilon))/\pi)^\omega((\alpha(3\zeta - 5x\varepsilon + 1/2x\vartheta(1 - x\zeta + x^2\varepsilon)))/\pi + (\beta 8^{\omega+1})/(8^\omega + ((3\zeta - 5x\varepsilon + 1/2x\vartheta(1 - x\zeta + x^2\varepsilon))/\pi)^\omega)))/\pi.$$

The occurrence of a reasonable number of unconstrained parameters (A, M, Q, p_r, R_c, α, β, ζ, ω, ε, ϑ) in the system (32) affirms that the matching criterion has met the needs of our study.

4. Star Quantities Relevant with Astronomical Observations

Based on physical grounds, it is essential to compute the star mass, radius and surface redshift for comparison with the geometrical features contained inside the stellar bodies. The calculated values have been presented in Tables 1–3.

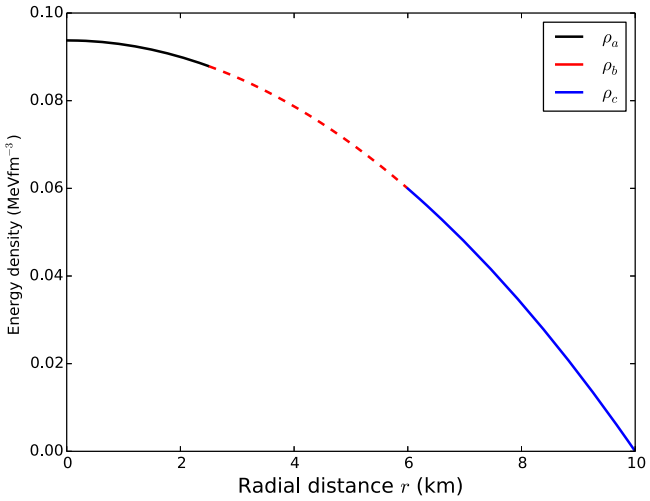

Figure 1. Energy density vs. radial distance.

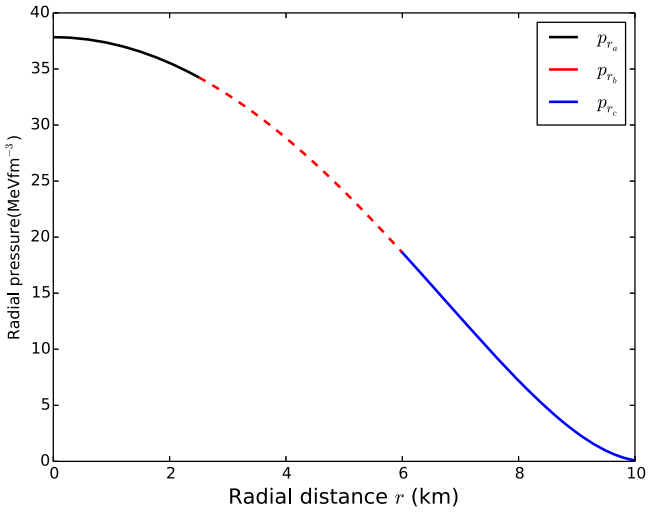

Figure 2. Radial pressure vs. radial distance.

5. Physical Conditions

To avoid discontinuity inside the star, matter variables, metric function and other physical viability must meet the following requirements:

(i) The energy density (ρ), and radial and transverse pressures (p_r, p_t) must be greater than zero, continuous, regular and defined throughout the interior of the star.

(ii) The metric functions $e^{-\lambda}$ and e^{ν} must be positive and unlimited throughout the interior.

(iii) The radial speed (ν) must be smaller than the speed of light to coincide with the causality limit $\frac{dp_r}{d\rho} < 1$ (Itoh 1970; Herrera 1992). In our study, we have computed in each layer as

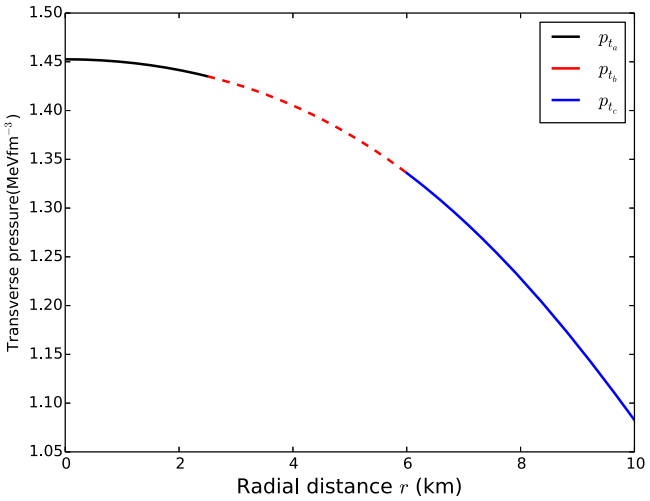

Figure 3. Transverse pressure vs. radial distance.

$$\nu_a = ((1+n)(16\pi)^{-1/n}(\zeta(4+x(2+x\vartheta)) - x(\vartheta+(8+x(2+x\vartheta))\varepsilon))^{1/n}\upsilon)/n, \tag{34a}$$

$$\nu_b = (8\pi N + \zeta(4+x(2+x\vartheta))\alpha - x(\vartheta+(8+x(2+x\vartheta))\varepsilon)\alpha)(8\pi)^{-1}, \tag{34b}$$

$$\begin{aligned}\nu_c = {} & (1/(\pi(\vartheta - 2x\zeta\vartheta - 10\varepsilon + 3x^2\vartheta\varepsilon)))2^{-2-3\omega} \\ & \times \pi((3\zeta - 5x\varepsilon + 1/2x\vartheta(1 \\ & - x\zeta + x^2\varepsilon))/\pi)^{\omega}((2^{3+4\omega}\beta(\vartheta - 2x\zeta\vartheta \\ & - 10\varepsilon + 3x^2\vartheta\varepsilon)((2^{(}1+3\omega)\pi \\ & - 2(-3+x)\zeta + x(\vartheta + 2(-5 \\ & + x)\varepsilon))/\pi)^{-\omega}\omega)/(\zeta(6 - x^2\vartheta) + x(\vartheta - 10\varepsilon \\ & + x^2\vartheta\varepsilon)) + 16^{1+\omega}\beta(2\zeta - \vartheta + 10\varepsilon - 4x\varepsilon) \\ & \times ((2^{1+3\omega}\pi + 6\zeta - 2x\zeta + x\vartheta \\ & + 2(-5+x)x\varepsilon)/\pi)^{-1-\omega}\omega \\ & + \alpha(\vartheta - 2x\zeta\vartheta - 10\varepsilon + 3x^2\vartheta\varepsilon)(1+\omega))/(2\pi)).\end{aligned} \tag{34c}$$

(iv) The energy conditions should be positive and continuous to satisfy the strong energy condition (SEC), the weak energy condition (WEC) and the null energy condition (NEC), i.e., SEC: $\rho - p_r - 2p_t \geqslant 0$, WEC: $\rho - 3p_t \geqslant 0$, $\rho - 3p_r \geqslant 0$, and NEC: $\rho - p_r \geqslant 0$, $\rho - p_t \geqslant 0$.

(v) Adiabatic index of imperfect fluid must agree with the critical stability criterion $\Gamma_{\rm crit} = \frac{\rho+p_r}{p_r}\frac{dp_r}{d\rho} \geqslant \frac{4}{3}$ (Maurya & Ortiz 2019). In our formulation, the computation of the condition in each layer has been done as follows:

$$\Gamma_a = ((1+n)(1+(16\pi)^{-1/n}(\zeta(4+x(2+x\vartheta)) - x(\vartheta+(8+x(2+x\vartheta))\varepsilon))^{1/n}\upsilon))/n, \tag{35a}$$

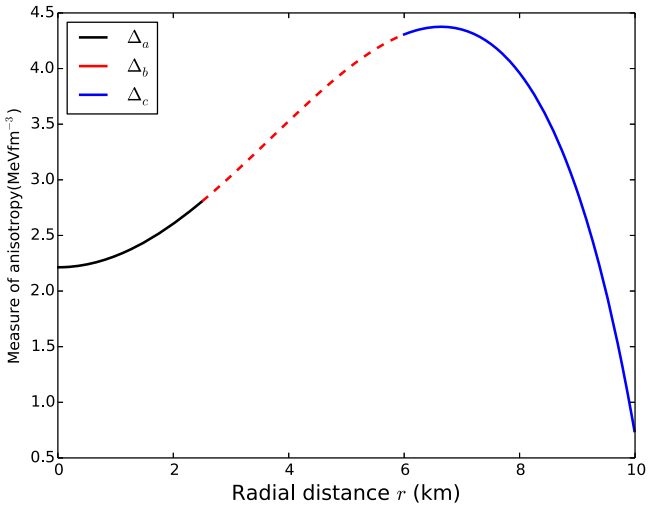

Figure 4. Measure of anisotropy vs. radial distance.

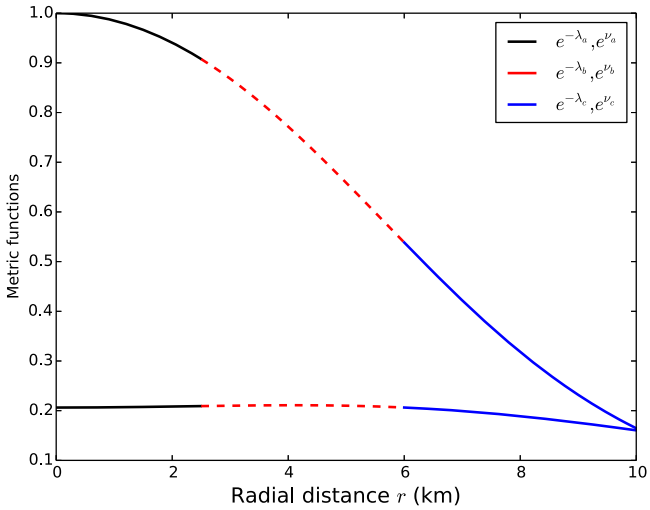

Figure 5. Metric functions vs. radial distance.

$$\begin{aligned}\Gamma_b = &((8\pi N + \zeta(4 + x(2 + x\vartheta))\alpha - x(\vartheta + (8\\ &+ x(2 + x\vartheta))\varepsilon)L)(-256\pi^2\Upsilon + 16\pi(1\\ &+ N)(\zeta(4 + x(2 + x\vartheta)) - x(\vartheta\\ &+ (8 + x(2 + x\vartheta))\varepsilon)) + (\zeta(4 + x(2 + x\vartheta)) - x(\vartheta\\ &+ (8 + x(2 + x\vartheta))\varepsilon))^2L))/(2048\pi^2 \quad (-\pi\Upsilon\\ &+ (((\zeta(4 + x(2 + x\vartheta)) - x(\vartheta + (8 + x(2\\ &+ x\vartheta))\varepsilon))(16\pi N + \zeta(4 + x(2 + x\vartheta))\alpha\\ &- x(\vartheta + (8 + x(2 + x\vartheta))\varepsilon)L))/(256\pi))),\end{aligned} \tag{35b}$$

Table 3
New Masses, Radii and Redshifts in Suitable Ranges

ζ	ϑ	ε	Radius	$M/M_\odot$	Redshift (Z_s)
0.12	0.86	1.9	9.1	2.612	3.13
0.20	0.76	1.9	8.9	1.193	2.83
0.28	0.66	1.9	9.2	1.095	3.06
0.36	0.64	1.9	8.6	1.273	2.11
0.44	0.56	1.9	9.9	1.498	2.75

(vi) In general relativity, the surface redshift has been thoroughly studied by many researchers from an astrophysical perspective (Gedela et al. 2019, 2021; Pant et al. 2020, 2021; Lighuda et al. 2021a, 2021b, 2023). Fewer authors have suggested that surface redshift must

$$\begin{aligned}\Gamma_c = &(2(3\zeta - 5x\varepsilon + 1/2x\vartheta(1 - x\zeta + x^2\xi)\\ &+ (8^{-2-\omega}((3\zeta - 5x\varepsilon + 1/2x\vartheta(1 - x\zeta\\ &+ x^2\varepsilon))/\pi)^{\omega}((\alpha(3\zeta - 5x\varepsilon + 1/2x\vartheta(1\\ &- x\zeta + x^2\varepsilon)))/\pi + 8^{1+\omega}\beta(8^{\omega} + (-2(-3\\ &+ x)\zeta + x(\vartheta + 2(-5 + x)\varepsilon))/(2\pi))^{-\omega}))/\pi)\\ &\times((2^{3+4\omega}\beta(\vartheta - 2x\zeta\vartheta - 10\varepsilon\\ &+ 3x^2\vartheta\xi)((2^{1+3\omega}\pi - 2(-3 + x)\zeta\\ &+ x(\vartheta + 2(-5 + x)\varepsilon))/\pi)^{-\omega}\omega)/(\zeta(6 - x^2\vartheta)\\ &+ x(\vartheta - 10\xi + x^2\vartheta\varepsilon)) + (16^{1+\omega}\beta(2\zeta - \vartheta + 10\varepsilon - 4x\xi)((2^{1+3\omega}\pi + 6\zeta - 2x\zeta\\ &+ x\vartheta + 2(-5 + x)x\varepsilon)/\pi)^{-1-\omega}\omega + \alpha(\vartheta - 2x\zeta\vartheta - 10\varepsilon + 3x^2\vartheta\varepsilon)(1 + \omega))/(2\pi)))/((\vartheta\\ &- 2x\zeta\vartheta - 10\varepsilon + 3x^2\vartheta\varepsilon)((\alpha(3\zeta - 5x\varepsilon\\ &+ 1/2x\vartheta(1 - x\zeta + x^2\varepsilon)))/\pi + 8^{1+\omega}\beta(8^{\omega}\\ &+ (-2(-3 + x)\zeta + x(\vartheta + 2(-5 + x)\varepsilon))/(2\pi))^{-\omega})).\end{aligned} \tag{35c}$$

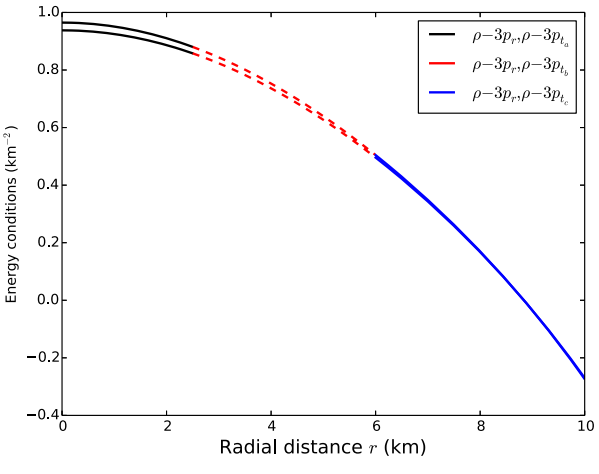

(a)

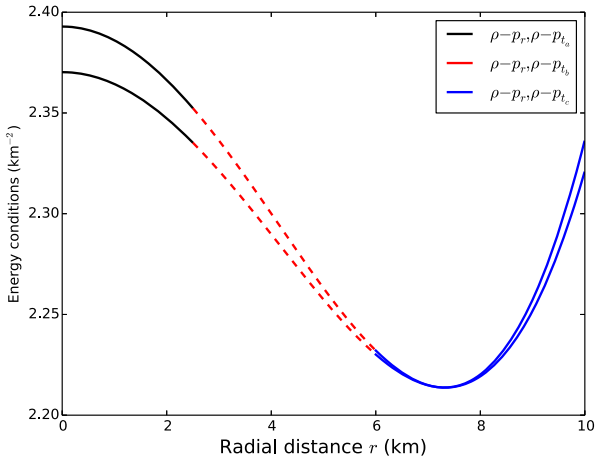

(b)

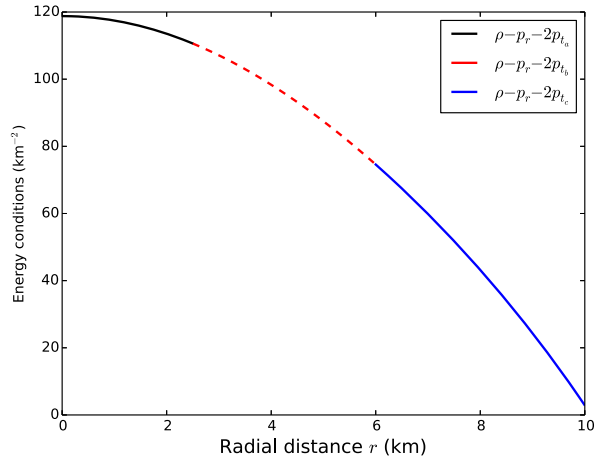

(c)

Figure 6. Energy conditions vs. radial distance.

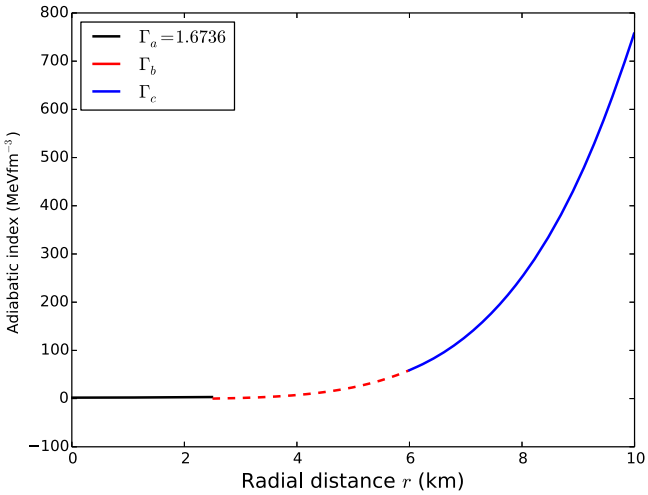

Figure 7. Adiabatic index vs. radial distance.

be less than 5.211 for imperfect fluids (Baraco & Hamity 2002; Ivanov 2002, 2010). The criterion for surface redshift is represented by

$$z_s = (1 - M(r))^{-1/2}, \tag{36}$$

where $M(r)$ is the efficient mass–radius ratio. In this study we have solved the redshift as follows

$$z_s = \Big(1 + \tfrac{1}{421}x(-42(10 + 3x)\zeta + 9x(7 - 5x\zeta)\vartheta + x(504 + 5x(18 + 7x\vartheta))\varepsilon)\Big)^{-1/2} - 1. \tag{37}$$

(vii) The compactification factor of dense stellar objects has been examined thoroughly in the study of astrophysical objects. The model developed by Jasim et al. (2018, 2020), Mathias et al. (2021), Jape et al. (2021) and Sunzu & Lighuda (2023) exhausted the mass–radius ratio of astrophysical objects in the interval (start 10^{-5} end 0.5) $M_{\odot}\,\mathrm{km}^{-1}$ for the group: normal stars, white dwarfs, neutron stars, ultra-dense compact stars and black holes. The compactification factor is expressed in the form $\Lambda(r) = \frac{2M_{\rm eff}}{r}$. Applying the criterion in this model produces

$$M(x) = \tfrac{1}{421}\sqrt{x}(42(10 + 3x)\zeta + 9x(-7 + 5x\zeta)\vartheta - x(504 + 5x(18 + 7x\vartheta))\varepsilon). \tag{38}$$

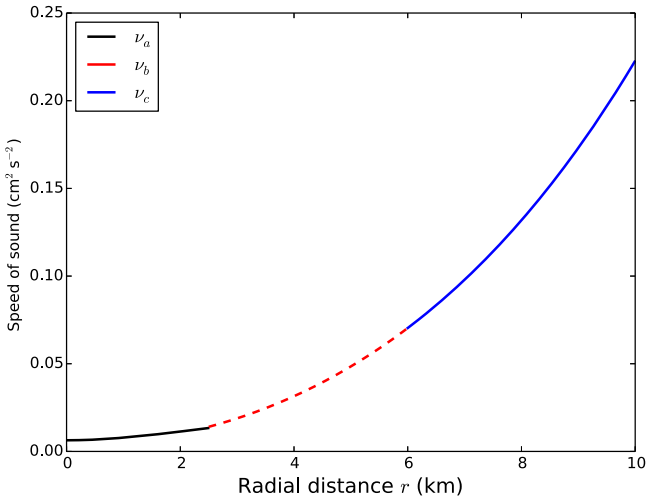

Figure 8. Radial speed vs. radial distance.

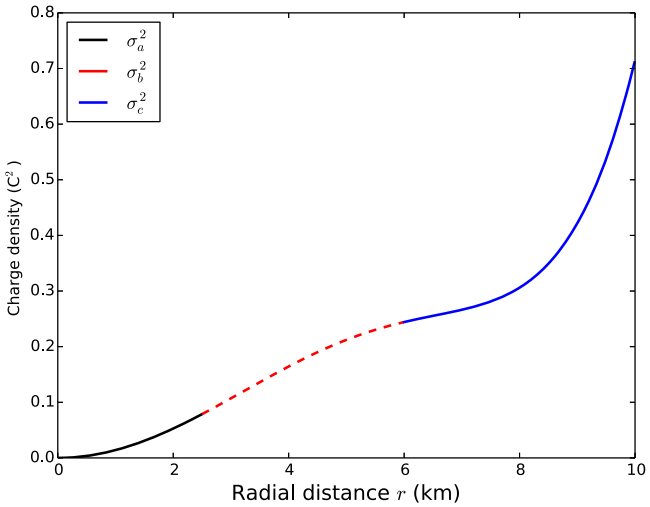

Figure 9. Charge density vs. radial distance.

(viii) Determination of the equilibrium forces in the study of the relativistic star has been enhanced by the Tolman–Oppenheimer–Volkoff (TOV) equation. Many authors have been applying the TOV equation to assess the viability of the matter configuration inside the star (Jasim et al. 2018, 2020; Maurya & Ortiz 2019; Maurya et al. 2019a, 2019b, 2019c, 2022; Jape et al. 2021; Mathias et al. 2021; Sunzu & Lighuda 2023). Referring to a charged object, the four equilibrium forces in the astrophysical study are gravitational force (F_g), anisotropic force (F_a), hydrostatic force (F_h) and electric force (F_e). The sum of equilibrium forces in general relativity must be zero: $F_g + F_a + F_h + F_e = 0$. The TOV equation is stated in the form

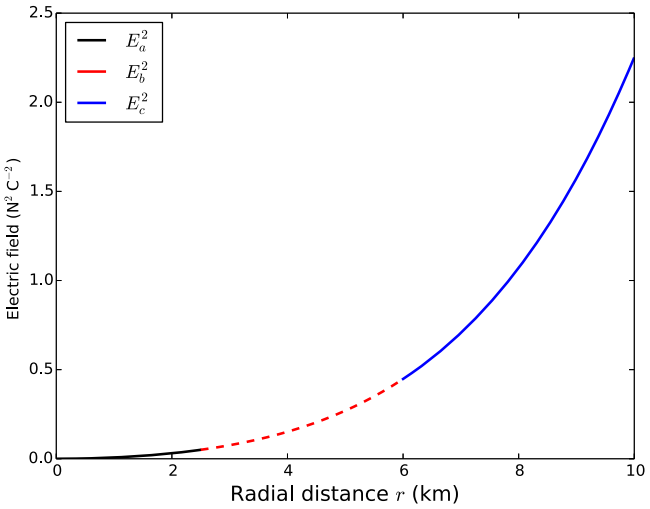

Figure 10. Electric field vs. radial distance.

$$-\frac{\nu'}{2}(\rho + p_r) - \frac{dp_r}{dr} + \frac{2}{r}(p_t - p_r) + \sigma E e^{-2\lambda} = 0. \quad (39)$$

In our treatment, we have calculated that

$$F_g = -\frac{\nu'}{2}(\rho + p_r), \quad (40a)$$

$$\begin{aligned} F_h &= -\frac{dp_r}{dr} \\ &= (1 + 1/n)(16\pi)^{(-1-1/n)}(6\zeta + 20x\zeta - \Upsilon \\ &\quad + x^2(-\zeta - 2x\zeta)\Upsilon + 2x(L - x(\zeta \\ &\quad + x\zeta))\Upsilon)(-2L + x(6\zeta + 10x\zeta - \Upsilon) \\ &\quad + x^2(L - x(\beta + x\zeta))\Upsilon)^{(1/n)}\vartheta, \end{aligned} \quad (40b)$$

$$F_a = \frac{2}{r}(p_t - p_r) = \frac{2}{r}\Delta, \quad (40c)$$

$$\begin{aligned} F_e &= \sigma E e^{-\lambda} \\ &= 2x\vartheta\sqrt{1/x - \zeta + x\varepsilon}\,(1 - x\zeta + x^2\varepsilon)^2 \\ &\quad \times (x\vartheta(1 - x\zeta + x^2\varepsilon) + \tfrac{1}{2}(3 \\ &\quad + (-2 + x\zeta)/(1 - x\zeta + x^2\varepsilon))). \end{aligned} \quad (40d)$$

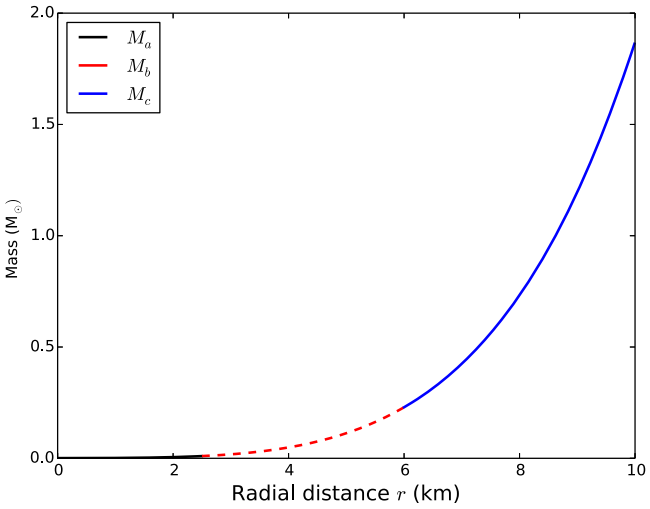

Figure 11. Mass vs. radial distance.

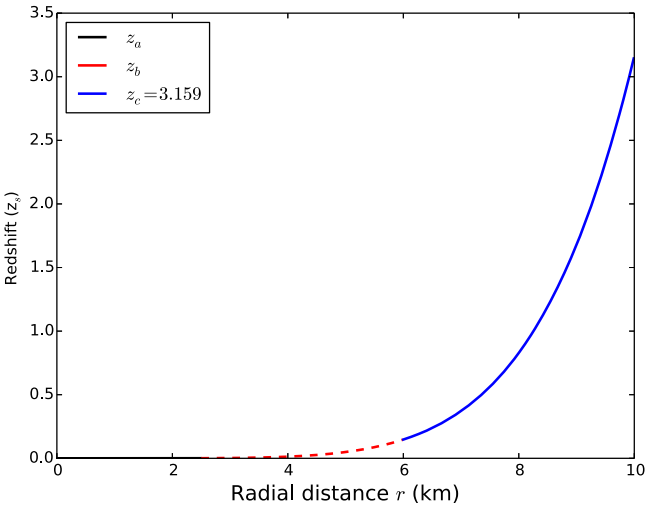

Figure 13. Redshift condition vs. radial distance.

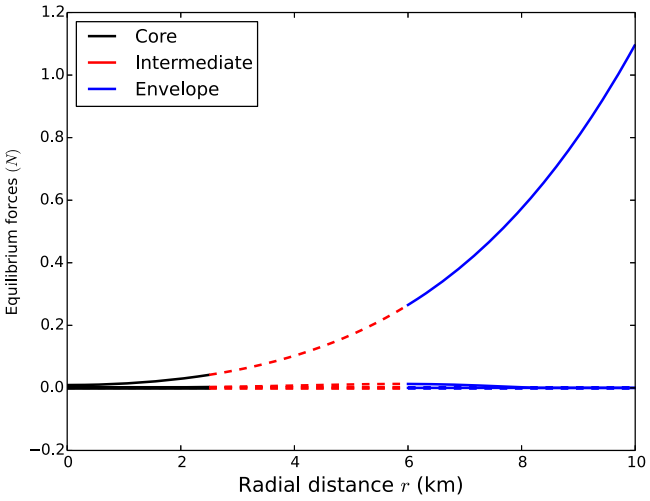

Figure 12. Variation of forces vs. radial distance.

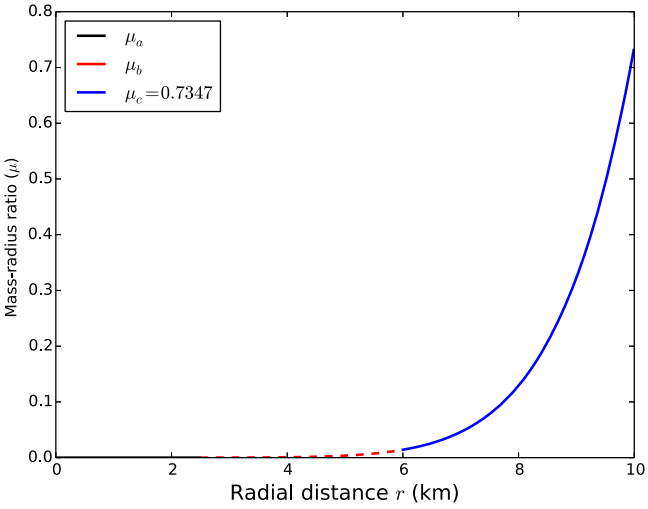

Figure 14. Mass–density ratio vs. radial distance.

6. Physical Analysis

In this paper, we have investigated the physical features inside the stars that comprise three layers with the inclusion of charge. The geometrical features are yielded in the range (0–2.5) km, (2.5–6.0) km and (6.0–10) km for the core region, intermediate region, and the envelope region respectively. The graphs for metric functions and matter variables are drawn versus radial distance in identified values of radius as applied in various studies done in the past (Gedela et al. 2019, 2021; Pant et al. 2020, 2021; Bisht et al. 2021; Mardan et al. 2021; Sunzu & Lighuda 2023; Mathias et al. 2024b). The graphs are obtainable by applying the specified values of the constants: $A = \pm 2.43$, $n = 3$, $L = \pm 0.47$, $\gamma = \pm 0.325$, $N = \pm 0.02 c_0 = c_1 = c_2 = 0.005$, $\alpha = \pm 0.000071$, $\beta = \pm 0.252$, $\Upsilon = 6.5$, $\zeta = \pm 0.0200$, $\upsilon = \pm 0.000148$, $\vartheta = \pm 0.0000685$ and $\varepsilon = \pm 0.675$.

Figures 1 and 2 affirm that the energy density and the radial pressure are maximum at the center, decreasing toward the enveloping layer. The same profiles are also found in the treatments of Pant et al. (2019, 2020), Gedela et al. (2019), Maharaj & Mafa Takisa (2013), Maharaj et al. (2014), Lighuda et al. (2021a, 2021b, 2023), Mardan et al. (2021) and Sunzu & Lighuda (2023). Figure 3 indicates the transverse pressure which demonstrates a decreasing profile. This physical trend is also marked in the study by Thirukkanesh & Maharaj (2008), Jape et al. (2021), Maurya et al. (2019a, 2019b, 2019c),

Mardan et al. (2021), Ngubelanga & Maharaj (2015) and Sunzu & Lighuda (2023). The measure of anisotropy in Figure 4 shows an increasing behavior, reaching a maximum peak where it starts to cease with the variation of the radial coordinate. We see that the behavior of anisotropy may be accelerated with the existence of the electric field and charge density. This viable characteristic is also demonstrated in the previous studies (Thirukkanesh & Ragel 2014; Murad 2016; Bhar et al. 2017; Pant et al. 2020, 2021; Bisht et al. 2021; Sunzu & Lighuda 2023). In Figure 5, the metric functions ($e^{-\lambda}$, e^{ν}) are observed to intersect at the boundary which is reasonable in the study of astrophysical objects (Lighuda et al. 2021a; Sunzu & Lighuda 2023; Mathias et al. 2024a, 2024b). Energy conditions in Figure 6 indicate the reducing behavior toward the enveloping layer which complies with the suggested criteria. These physical treads are also seen in the models by Gedela et al. (2019, 2021), Mafa Takisa et al. (2019), Lighuda et al. (2021a), Mardan et al. (2021) and Mathias et al. (2021). Figure 7 represents the adiabatic index utilized to measure the stability condition of the stars ($\Gamma \geqslant 4/3$). In our model, we yield $\Gamma_{x=0} = 1.6736$ which affirms that the star is stable versus gravitationally abrupt. A similar physical trend is also captured in Mathias et al. (2024a, 2024b), Sunzu & Lighuda (2023), Jasim et al. (2018, 2020), and Jape et al. (2021). Figure 8 affirms that the radial speed of sound has less range than the speed of light. In our study, we obtained values in the range ($0.00798 \leqslant \nu \leqslant 0.225$) which is acceptable in the star. The same trend was also observed in various models constructed in the past (Gedela et al. 2019, 2021; Mafa Takisa et al. 2019; Pant et al. 2019, 2021; Mathias et al. 2021; Lighuda et al. 2023; Sunzu & Lighuda 2023). Figures 9 and 10 illustrate the charge density and electric field respectively. The two graphs of σ^2 and E^2 experience an increasing behavior away from the physically acceptable center. Figure 11 indicates that the mass function is becoming larger from the origin toward the surface, which is consistent with the study of relativistic stars. In Figure 12, we observe the hydrostatic force (F_h), the electric force (F_e) and the gravitational force (F_g) are coming forth: flowing uniformly toward the surface where an anisotropic force (F_a) seems to increase. This can also be demonstrated in the work of Fulara & Sah (2018), Lighuda et al. (2021a), Das et al. (2016), Jape et al. (2021), Mathias et al. (2021) and Sunzu & Lighuda (2023). Figure 13 depicts that the redshift is monotonically increasing versus radial coordinate (r) having the maximum value $z_s = 3.159$ which is true in general relativity. We can also find this trend in the study of Lighuda et al. (2021b), Maurya & Ortiz (2019), Maurya et al. (2019a, 2019b, 2019c, 2022) and Jasim et al. (2018, 2020). Figure 14 depicts the trend of the mass–radius ratio as an increasing function, reaching the peak value $\mu(x) = 0.7347$ which is consistent in the study of the stars.

7. Conclusion

In our paper, we have yielded a new solution utilizing the Einstein–Maxwell system of differential equations. Our model comprises three interior layers: each satisfying a chosen EoS. Matching across the layers has been gently completed by utilizing exterior Reissner–Nordström spacetime. A deep analysis of the physical features has been exhausted, affirming that all physical parameters are feasible and consistent with the study of massive stellar objects. Our solution is an extension of the two-layered model developed by Sunzu & Lighuda (2023) into a three-layered model: yielding notable geometrical features in the third layer fitted with a modified Van der Waals EoS. These are physically demonstrated in various graphs. Next time, we shall construct a charged model that will obey distinguishable multi-layered settings.

References

Abreu, H., Hernandez, H., & Nunez, L. A. 2007, CQGra, 24, 4631
Baraco, D. E., & Hamity, V. H. 2002, PhRvD, 65, 124028
Bhar, P., Singh, K. N., & Pant, N. 2017, InJPh, 91, 6
Bhatia, M. S., Bonazzola, S., & Szamosi, G. 1969, A&A, 3, 206
Bijalwan, N. 2011, Ap&SS, 336, 413
Bisht, R. K., Gedela, S., Pant, N., & Tewari, N. 2021, RAA, 21, 162
Bonnor, W. B. 1960, ZPhy, 160, 59
Das, A., Rahaman, F., Guha, B. K., & Ray, S. 2016, EPJC, 76, 654
Durgapal, M. C., & Bannerji, R. 1982, Ap&SS, 84, 409
Durgapal, M. C., & Bannerji, R. 1983, PhRvD, 27, 328
Fulara, P. C., & Sah, A. 2018, IJAA, 8, 46
Gedela, S., Bisht, R. K., & Pant, N. 2018, EPJA, 54, 207
Gedela, S., Pant, N., Upreti, J., & Pant, R. P. 2019, EPJC, 79, 566
Gedela, S., Pant, N., Upreti, J., & Pant, R. P. 2021, EPJP, 36, 215005
Hansraj, S., Maharaj, S. D., & Mlaba, S. 2016, EPJP, 131, 4
Herrera, L. 1992, PhLA, 165, 206
Ipser, J. R. 1969, ApJ, 158, 17
Itoh, N. 1970, PThPh, 1, 44
Ivanov, B. V. 2002, PhRvD, 65, 104001
Ivanov, B. V. 2010, IJTP, 49, 1236
Jape, J. W., Maharaj, S. D., Sunzu, J. M., & Mkenyeleye, J. M. 2021, EPJC, 81, 1057
Jasim, M. K., Deb, D., Ray, S., Gupta, Y. K., & Chowdhury, S. R. 2018, EPJC, 78, 603
Jasim, M. K., Maurya, S. K., & Al-Sawaii, A. S. M. 2020, Ap&SS, 365, 9
Komathiraj, K., & Maharaj, S. D. 2007, IJMPD, 16, 1803
Kumar, J., Maurya, S. K., Prasad, A. K., & Banerjee, A. 2019, JCAP, 11, 005
Lighuda, A. S., Maharaj, S. D., Sunzu, J. M., & Mureithi, E. W. 2021a, Ap&SS, 366, 76
Lighuda, A. S., Maharaj, S. D., Sunzu, J. M., & Mureithi, E. W. 2023, Prama, 97, 5
Lighuda, A. S., Sunzu, J. M., Maharaj, S. D., & Mureithi, E. W. 2021b, RAA, 21, 310
Mafa Takisa, P., & Maharaj, S. D. 2016, Ap&SS, 361, 262
Mafa Takisa, P., Maharaj, S. D., & Mulangu, C. 2019, Prama, 92, 40
Maharaj, S. D., & Mafa Takisa, P. 2013, GeReGr, 45, 1951
Maharaj, S. D., Sunzu, J. M., & Ray, S. 2014, EPJP, 129, 3
Malaver, M. 2017a, WSN, 86, 333
Malaver, M. 2017b, WSN, 86, 1
Makalo, P. D., Sunzu, J. M., & Mkenyeleye, J. M. 2022, NewA, 98, 10135
Mardan, S. A., Noureen, I., & Khalid, A. 2021, EPJC, 81, 912
Mathias, A. K., Maharaj, S. D., Sunzu, J. M., & Mkenyeleye, J. M. 2021, Prama, 95, 178
Mathias, A. V., Mkenyeleye, J. M., & Sunzu, J. M. 2024b, NewA, 110, 102216
Mathias, A. V., Sunzu, J. M., & Mkenyeleye, J. M. 2024a, NewA, 106, 1012115

Maurya, S., Govender, M., Singh, K. N., & Nag, R. 2022, EPJC, 82, 49
Maurya, S. K., Banerjee, A., Jasim, M. K., et al. 2019a, PhRvD, 99, 044029
Maurya, S. K., Errehymy, A., Deb, D., Tell-Ortiz, F., & Daoud, M. 2019c, PhRvD, 100, 044014
Maurya, S. K., Maharaj, S. D., Kumar, J., & Prasad, A. K. 2019b, GeReGr, 51, 86
Maurya, S. K., & Ortiz, F. T. 2019, EPJC, 79, 85
Metcalfe, T. S., Montgomery, M. H., & Kawaler, S. D. 2003, MNRAS, 344, L88
Misner, W. C., Thorne, S. K., & Wheeler, A. J. 1973, Gravitation (San Francisco, CA: Freeman)
Montgomery, M. H., Metcalfe, T. S., & Winget, D. E. 2003, MNRAS, 344, 657
Murad, M. H. 2016, Ap&SS, 361, 20
Ngubelanga, S. A., & Maharaj, S. D. 2015, EPJP, 130, 211
Ngubelanga, S. A., Maharaj, S. D., & Ray, S. 2015, Ap&SS, 357, 74
Olengeile, L., Sunzu, M. J., & Mkenyeyele, M. J. 2023, NewA, 100, 102002
Oppenheimer, J. R., & Volkoff, G. M. 1939, PhRv, 55, 374
Pant, N., Gedela, S., Pant, R. P., Upreti, J., & Bishi, R. K. 2020, EPJP, 135, 180
Pant, N., Govender, M., & Gedela, S. 2021, RAA, 21, 109
Pant, R. P., Gedela, S., Bisht, R. K., & Pant, N. 2019, EPJC, 79, 602
Rahaman, F., Ray, S., Jafry, A. K., & Chakraborty, N. 2010, PhRvD, 82, 104055
Ramesh, T., & Thomas, V. O. 2005, Prama, 64, 5
Sharma, R., & Maharaj, S. D. 2007, MNRAS, 375, 1265
Sharma, R., & Mukherjee, S. 2002, MPLA, 17, 2535
Sunzu, J. M., & Lighuda, A. S. 2023, NewA, 100, 101977
Sunzu, J. M., Maharaj, S. D., & Ray, S. 2014a, Ap&SS, 1, 634
Sunzu, J. M., Maharaj, S. D., & Ray, S. 2014b, Ap&SS, 352, 719
Sunzu, J. M., & Mashiku, T. 2018, Prama, 91, 75
Sunzu, J. M., Mathias, A. K., & Maharaj, S. D. 2019, JApA, 40, 8
Thirukkanesh, S., & Maharaj, S. D. 2008, CQGra, 25, 235001
Thirukkanesh, S., & Maharaj, S. D. 2009, MMAS, 32, 684
Thirukkanesh, S., & Ragel, F. C. 2014, Ap&SS, 81, 1
Thomas, V. O., Ratanpal, B. S., & Vinodkumar, P. C. 2005, IJMPD, 14, 85
Tikekar, R., & Jotania, K. 2009, GrCo, 15, 129
Varela, V., Rahaman, F., Ray, S., Chakraborty, K., & Kalam, M. 2010, PhRvD, 82, 044052